



# Chandra Observations of Six Peter Pan Disks: Diversity of X-Ray-driven Internal Photoevaporation Rates Does Not Explain Their Rare Longevity

Stefan Laos<sup>1</sup> , John P. Wisniewski<sup>1</sup> , Marc J. Kuchner<sup>2</sup> , Steven M. Silverberg<sup>3</sup> , Hans Moritz Günther<sup>3</sup> ,  
David A. Príncipe<sup>3</sup> , Brett Bonine<sup>1</sup>, and Marina Kounkel<sup>4</sup>   
The Disk Detective Collaboration

<sup>1</sup>Homer L. Dodge Department of Physics and Astronomy, University of Oklahoma, 440 West Brooks Street, Norman, OK 73019, USA

<sup>2</sup>NASA Goddard Space Flight Center, Exoplanets and Stellar Astrophysics Laboratory, Code 667, Greenbelt, MD 20771, USA

<sup>3</sup>MIT Kavli Institute for Astrophysics and Space Research, 77 Massachusetts Avenue, Cambridge, MA 02139, USA

<sup>4</sup>Department of Physics and Astronomy, Vanderbilt University, VU Station 1807, Nashville, TN 37235, USA

Received 2022 April 23; revised 2022 June 22; accepted 2022 July 13; published 2022 August 22

## Abstract

We present Chandra X-ray observations of six previously identified Peter Pan objects, rare  $\sim 40$  Myr systems with evidence of primordial disk retention. We observe X-ray luminosities (0.8–3.0 keV) ranging from  $\log L_x \sim 27.7$ –29.1. We find that our Peter Pan sample exhibits X-ray properties similar to that of weak-lined T Tauri stars and do not exhibit evidence of stellar accretion induced X-ray suppression. Our observed Peter Pan X-ray luminosities are consistent with that measured for field dM stars of similar spectral type and age, implying their long primordial disk lifetimes are likely not a consequence of unusually faint X-ray host stars. Our derived X-ray photoevaporative mass-loss rates predict our systems have passed the point of rapid gas dispersal and call into question the impact of this internal mechanism for primordial disk dispersal around dM stars. Our qualitative assessment of the surrounding Peter Pan environments also does not predict unusually low levels of external photoevaporation relative to other respective moving group members. Overall, our results suggest Peter Pan disks may be a consequence of the low far-UV flux incident on the disk in low-mass dM stars given their relatively lower levels of accretion over the course of their pre-main-sequence evolution.

*Unified Astronomy Thesaurus concepts:* X-ray astronomy (1810); Circumstellar disks (235); Low mass stars (2050)

## 1. Introduction

Large, sensitive IR surveys conducted by NASA’s Spitzer and WISE satellites have demonstrated both that primordial protoplanetary disks of dust and gas clear on rapid ( $\lesssim 10$  Myr) timescales, and that this dissipation timescale depends on the mass of the host protostar (Carpenter et al. 2006; Wahhaj et al. 2010; Pecaut & Mamajek 2016). Although dispersion exists between different environments, the FEPS and c2d legacy Spitzer surveys have found that  $\sim 10$  Myr is an upper limit for the lifetimes of primordial disks around solar-type stars (Carpenter et al. 2006; Wahhaj et al. 2010; Williams & Cieza 2011). For lower-mass K-type stars, the frequency of primordial disks is  $\sim 9\%$  at 10 Myr and  $\sim 4\%$  by 16 Myr, indicating a disk e-folding timescale of  $\sim 4$ –5 Myr (Pecaut & Mamajek 2016). These disk lifetimes not only set the timescale for the star formation process but also necessarily constrain the timescale for planet formation in these systems. Understanding the detailed evolution of primordial disks around the most abundant low-mass stars (e.g., M dwarfs) is of strong current interest, due in part to the expected windfall of M-dwarf planet science from NASA’s TESS mission. TESS has already confirmed 18 planets having radii less than  $2 R_{\oplus}$  surrounding low-mass M dwarfs (e.g., Crossfield et al. 2019; Demangeon et al. 2021).

Once depleted of gas, primordial disks evolve into second-generation debris disks. They are composed primarily of dust, created by continuous collisional destruction of cometary and asteroidal bodies that are remnants of the star and planet formation process. This destruction is thought to be at least partially stirred by the presence of planetary bodies in the system (Wyatt 2008). These systems have depleted most of their gas and no longer exhibit signatures of accretion. The frequency of debris can be as high as 20% for young main-sequence A-type stars, and such disks can persist for hundreds of Myr (Rieke et al. 2005). By contrast, Binks (2016) found zero M-dwarf debris disks in their ALLWISE study of moving groups older than 40 Myr, consistent with the small number of candidate M-dwarf debris disk systems identified by Theissen & West (2014) (of which some were false-positive detections; Silverberg et al. 2018). The observed low frequency of old ( $\geq 40$  Myr) M-dwarf debris disks may indicate that such systems are ultimately cleared by stellar wind (Wyatt 2008) or stellar activity (e.g., AU Mic; Grady et al. 2020) over shorter timescales.

Over the past few years, a new population of low-mass, M-type stars, with ages  $\sim 45$  Myr reliably secured via moving group membership, have been found to exhibit substantial ( $L_{IR}/L_{*} \sim 0.1$ ) mid-IR excesses, indicative of the presence of warm dust disks (Boucher et al. 2016; Silverberg et al. 2016; Murphy et al. 2018; Lee et al. 2020; Silverberg et al. 2020). While such systems were initially interpreted to be (rare) examples of the oldest dM-type debris disk systems (Silverberg et al. 2016), their large IR excesses suggest there should be gas in the system, and is less consistent with the interpretation of a debris disk origin. Indeed, growing evidence shows some of these systems exhibit clear accretion



Original content from this work may be used under the terms of the [Creative Commons Attribution 4.0 licence](https://creativecommons.org/licenses/by/4.0/). Any further distribution of this work must maintain attribution to the author(s) and the title of the work, journal citation and DOI.

**Table 1**  
Peter Pan X-Ray Observations

Object	Obs. Date (UTC)	Obs. ID	Exposure (ks)
WISEA J094900.65-713803.1 A/B	12/13/2019 15:34	22305	17
2MASS J05010082-4337102	12/22/2019 5:15	22306	19
WISEA J044634.16-262756.1 A/B	5/20/2020 4:48	22304	22
	5/21/2020 8:57	23255	10
	6/2/2020 4:27	23256	23
	7/6/2021 14:29	22303	36
WISEA J080822.18-644357.3	7/6/2021 14:29	22303	36
	7/7/2021 6:24	24756	35

tracers, with strong (10–125 Å), broad (200–350 km s<sup>-1</sup>) H $\alpha$  emission (Boucher et al. 2016; Murphy et al. 2018; Silverberg et al. 2020) and variable Paschen  $\beta$  and Brackett  $\gamma$  emission (Silverberg et al. 2020) in the canonical case of WISEA J080822.18-644357.3. With evidence of ongoing gas accretion despite their significantly advanced ages, this set of objects have been coined as “Peter Pan” objects, given their refusal to “grow up” (Silverberg et al. 2020). These systems may also be the precursors to notable systems like TRAPPIST-1 (Gillon et al. 2017), in which a long-surviving disk around a low-mass dM star circularizes numerous planetary orbits into a stable configuration.

Overall, these systems currently challenge the standard paradigm for primordial disk (and planet formation) lifetimes. Silverberg et al. (2020) argue the simplest explanation for these systems is that they are primordial disks that are still in the process of dissipating, implying lower than average disk gas mass-loss rates. A key driver of primordial disk dissipation is photoevaporation of the disk’s gas content from high energy photons radiated by the host star (Hollenbach et al. 1994; Clarke et al. 2001; Alexander et al. 2004; Font et al. 2004; Ercolano et al. 2009; Gorti & Hollenbach 2009; Owen et al. 2010; Williams & Cieza 2011). Studies of the low-mass population of the TW Hya association have shown an anticorrelation between X-ray luminosity and disk fraction as a function of spectral type; earlier M dwarfs have higher X-ray luminosities and a lower disk fraction than mid-late M dwarfs (Kastner et al. 2016). The fundamental question remains: are the disks around Peter Pan stars primordial and if so, why have they persisted around these dwarf M stars and not others? Do Peter Pan objects represent a rare class of X-ray faint stars?

We investigate these open questions with our new X-ray observations, which gauge the soft (0.8–3.0 keV) X-ray photons radiating from the host star. In this paper, we characterize the X-ray properties of identified Peter Pan objects and estimate their expected mass-loss rates from X-ray driven photoevaporation for the first time. In Section 2, we describe the nature of our Chandra observations as well as our utilized data reduction and spectral extraction techniques. In Section 3, we report our derived Peter Pan X-ray luminosities, comparing to both active, young stars and also other dwarf M-type stars in nearby moving groups. We also compare our findings to the X-ray luminosities used in the recent modeling of Wilhelm & Portegies Zwart (2022). In Section 4, we interpret these observations in the context of recent modeling and proposed disk dispersal processes. Finally, in Section 5, we conclude with a brief summary of our findings.

## 2. Observations and Data Reduction

X-ray observations (Table 1) of our Peter Pan sample were obtained with the Advanced CCD Imaging Spectrometer

(ACIS) on board the Chandra X-ray Observatory. All data were acquired on ACIS-S3 chip in VFaint mode.

To extract our X-ray spectra, we analyzed the pipeline-processed data files provided by the Chandra X-ray Center using standard science threads with CIAO version 4.13 and calibration data from CALDB version 4.9.5 (Fruscione et al. 2006). Spectra were extracted using circular apertures centered on the stellar X-ray sources, with diameters of 4'' in the case of J0501 and J0808. In the case of close binaries J0949 ( $a \sim 1''.5$ ) and J0446 ( $a \sim 2''.3$ ), we closely inspect the binned level 2 event files by eye, adopting optimal aperture diameters of  $\sim 1''.4$  and  $\sim 2''.6$ , respectively. These sizes minimized companion contamination while also maximizing the enclosed energy fraction given the Chandra on-axis point-spread function. For each observation, we sample the background with a circular aperture in a nearby region on the same CCD to each source.

To derive X-ray luminosities for our Peter Pan sample, we analyze our observed X-ray spectra (Section 2) using version 4.13 of CIAO/SHERPA (Doe et al. 2007) and version 4.9.5 of CALDB (Fruscione et al. 2006). We note our X-ray count data peak around 1 keV for all objects, expected from their young, pre-main-sequence status. For each individual observation, we group the data to 5 counts per bin and consider counts in the 0.8–3 keV range for fitting. For our spectral model, we adopt the XSPEC optically thin plasma model `vapex`, considering only a single temperature component to avoid over-fitting our low-count data. We also add a multiplicative photoelectric absorption component `wabs` to our spectral model. We find negligible intervening absorption, expected given the close proximity of our sources ( $\lesssim 100$  pc), and choose to freeze its value to zero.

Similar to the analysis done in Kastner et al. (2016), we fix our plasma abundances to the typical values determined for T Tauri stars in Taurus (Skinner & Güdel 2013 and references therein). Relative to solar, these abundance values are H = 1.0, He = 1.0, C = 0.45, N = 0.79, O = 0.43, Ne = 0.83, Mg = 0.26, Al = 0.50, Si = 0.31, S = 0.42, Ar = 0.55, Ca = 0.195, Fe = 0.195, and Ni = 0.195. In the case of J0446A/B and J0808, we perform simultaneous fits over the numerous observations of each object. To gauge the quality of our fits, we consider the Cash statistic (Cash 1979) as implemented in SHERPA rather than a chi-squared metric, which is not appropriate for the Poisson-distributed low-count regime of our data. The resulting best-fit parameters derived from this analysis are given in Table 2. From these best fits, we derive X-ray fluxes in the 0.3–8 keV energy band and use Gaia DR3 distances (Gaia Collaboration et al. 2021) to derive our Peter Pan X-ray luminosities ( $L_x$ ), also reported in Table 2. Our best fits are shown in Appendix A. Given the low count rates and correspondingly large relative Poisson uncertainty, we note we

**Table 2**  
X-Ray Spectral Analysis: Best-fit Parameters

Source	$F_x$ ( $\text{erg s}^{-1} \text{cm}^{-2}$ )	kT (keV)	Norm	Reduced Cstat <sup>a</sup>	$L_x$ ( $\text{erg s}^{-1}$ )	$L_{\text{bol}}$ ( $\text{erg s}^{-1}$ )	Spectral Type <sup>b</sup>	Age (Myr)
J0949A	$1.5 \pm 0.4\text{E-}13$	$0.28 \pm 0.02$	$3.0\text{E-}4 \pm 7.5\text{E-}5$	1.69	$1.10\text{E+}29$	$1.10\text{E+}32$	M4	45
J0949B	$6.6 \pm 0.9\text{E-}14$	$0.73 \pm 0.13$	$8.4\text{E-}5 \pm 1.5\text{E-}5$	1.39	$4.80\text{E+}28$	$9.60\text{E+}31$	M5	45
J0501	$2.1 \pm 0.6\text{E-}14$	$0.63 \pm 0.28$	$2.0\text{E-}5 \pm 9.2\text{E-}6$	1.49	$5.90\text{E+}27$	$2.60\text{E+}31$	M4.5	42
J0446A	$4.39 \pm 0.4\text{E-}14$	$0.95 \pm 0.09$	$3.8\text{E-}5 \pm 3.4\text{E-}6$	1.05	$3.60\text{E+}28$	$5.24\text{E+}32$	M6	42
J0446B	$3.03 \pm 0.9\text{E-}14$	$0.50 \pm 0.10$	$2.7\text{E-}5 \pm 6.3\text{E-}6$	1.65	$2.50\text{E+}28$	$5.19\text{E+}32$	M6	42
J0808	$1.21 \pm 0.4\text{E-}14$	$0.46 \pm 0.12$	$1.1\text{E-}5 \pm 3.7\text{E-}6$	0.77	$1.50\text{E+}28$	$3.07\text{E+}31$	M5	45

**Notes.**

<sup>a</sup> The Cstat procedure is the XSPECa implementation of the Cash statistic (Cash 1979), which also incorporates fitting a model to the background. The reduced Cstat values correspond to the observed statistic divided by the degrees of freedom, operating as an approximate goodness-of-fit metric with good fits to the data approaching a nominal value of 1.

<sup>b</sup> Spectral types are derived from the analysis of Silverberg et al. (2020) and references therein. Ages are estimated from the isochronal fitting of Bell et al. (2015).

cannot exclude variability of a factor of 2 between our observations, but would have detected order-of-magnitude flares had they occurred during our observations.

To compute overall fractional luminosities, we also compute the bolometric luminosity of our Peter Pan sources. Following the methodology of Kastner et al. (2016), we use known spectral types, Gaia DR3 distances, and *J*-band data based on the (spectral-type-dependent) *J*-band bolometric corrections determined by Pecaut & Mamajek (2013) assuming no reddening. For spectral types later than M5, we linearly extrapolate from the bolometric *J* correction relation. In the cases of J0446 and J0949, we assume the flux contribution from each stellar component is equal. These values are reported in Table 2.

### 3. Results

With our derived luminosities, we explore the X-ray properties of our six Peter Pan targets for the first time. In Section 3.1, we consider our X-ray luminosities in the context of stellar accretion. In Section 3.2, we compare our derived values to sensitive X-ray observations of our M-star analog control sample (Appendix B). We also compare our luminosities to that utilized in the prescriptions of recent modeling in Section 3.3.

#### 3.1. Accretion versus $L_x$

We begin by comparing our sample with the large sample of classical and weak-lined T Tauri stars (CTTSs, WTTSs) in Taurus from Telleschi et al. (2007). The sensitive XMM-Newton observations of this young (average age of  $\sim 2.4$  Myr), active sample allow us to further gauge the impact of active stellar accretion on  $L_x$ .

Probing even lower bolometric luminosities, our observations find a large diversity in  $L_x$  across the Peter Pan sample (Figure 1), spanning a range of  $\sim 1.5$  dex. Their overall appreciable X-ray luminosities do not show evidence for the significant ( $\sim 2\times$ ) X-ray suppression seen in the (actively accreting) CTTS subsample (Telleschi et al. 2007). We instead find the  $L_x/L_{\text{bol}}$  values of the Peter Pan sources more closely follow the trend observed in the WTTSs, consistent with the similarly weak level of Peter Pan accretion ( $\sim 10^{-11}$ – $10^{-9} M_{\odot} \text{yr}^{-1}$ ) derived from recent H $\alpha$  observations Silverberg et al. (2020).

We also compare the H $\alpha$  emission equivalent widths from the measurements of Silverberg et al. (2020) with our observed X-ray luminosities. We do not find evidence of a strong correlation (computing a Pearson correlation coefficient value of  $-0.45$ ) within the limitations of our small sample. Interestingly, we note

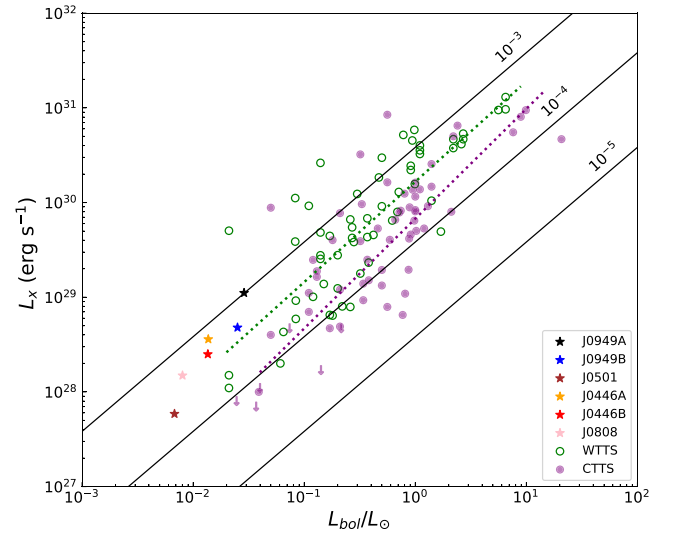


**Figure 1.** Comparison of observed X-ray luminosities between our Peter Pan sample (starred points) and the T Tauri stars from Telleschi et al. (2007). Upper limits are indicated with arrows. Diagonal black lines represent constant X-ray to bolometric luminosity fractions ( $L_x/L_{\text{bol}}$ ) of  $10^{-3}$ ,  $10^{-4}$ ,  $10^{-5}$ . Linear regressions for the WTTS (green) and CTTS (purple) subsamples are reproduced from Telleschi et al. (2007), shown as dotted lines. We find the Peter Pan sources more closely resemble the  $L_x/L_{\text{bol}}$  behavior exhibited by the WTTSs (green) relative to the X-ray fainter CTTSs (purple).

the strongest accretor (J0949A) is also our brightest X-ray object, counter to the expectation from stellar accretion induced X-ray suppression. Collectively, these results do not find evidence of significant X-ray suppression in the Peter Pan sample as seen in the active CTTSs, likely due to their relatively low level of accretion.

#### 3.2. M-star Control Sample Comparison

Our comparison with the T Tauri stars from (Telleschi et al. 2007) in Section 3.1 mainly considers relatively young stars ( $\sim 1$ – $10$  Myr). Given the suspected advanced ages of the Peter Pan sources ( $\sim 45$  Myr; Silverberg et al. 2020), we construct a new comparison sample, closely matching suspected spectral types and ages with similarly sensitive X-ray observations. We describe our control sample criteria in Appendix B.

In Figure 2, we compare both X-ray (left panel) and fractional X-ray (right panel) luminosities between our Peter Pan sources and this control sample. Overall, we find the values

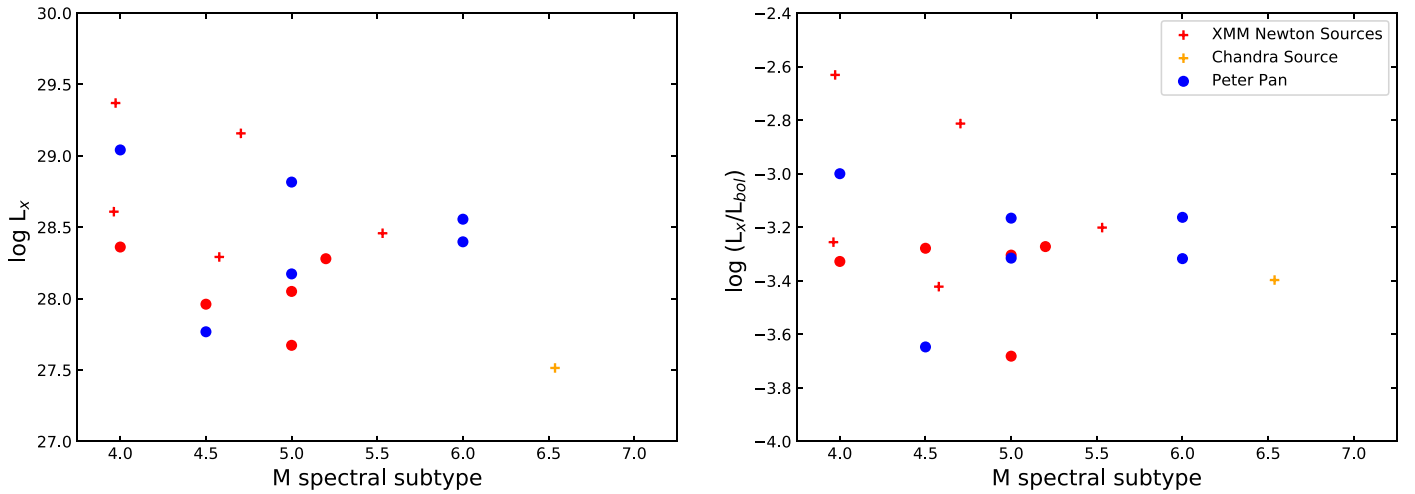


**Figure 2.** Observed X-ray (left) and fractional X-ray (right) luminosities as a function of spectral type between the Peter Pan sample and M-star control sample (i.e., similar ages and spectral types of our Peter Pan sample). Circular points represent spectroscopically verified spectral types while crosses represent spectral types estimated via colors. Overall, we find our derived Peter Pan luminosities to be consistent with that observed for other moving group M stars.

observed are consistent with one another. We therefore do not find evidence that these known Peter Pan sources are over- or underluminous in X-rays relative to similarly evolved M stars. This finding may argue against the previously thought rarity of disk longevity out to Peter Pan ages for mid-M types. We explore this possibility further in Section 4.

### 3.3. Predicted versus Observed X-Ray Luminosity Evolution in $dM$ Stars

Our X-ray observations offer a set of measurements to benchmark the characteristic X-ray luminosity for Peter Pan disk systems and assess previously used predictions. Recent modeling has investigated the survival of primordial circumstellar disks out to the advanced ages of 45 Myr (Wilhelm & Portegies Zwart 2022), assuming disk winds from strong stellar X-rays constitute the primary internal source of disk dispersal. Detailed simulations of this mass-loss procedure (Owen et al. 2012; Picogna et al. 2019) have found a power-law dependence on the X-ray luminosity of the host star (which in turn is dependent on stellar mass).

To estimate the expected Peter Pan X-ray luminosity, Wilhelm & Portegies Zwart (2022) consider the characteristic (quiescent) X-ray luminosity–mass relation derived by Flaccomio et al. (2012) for young stars observed by the Chandra Orion Ultra Deep Project (Getman et al. 2005), which is nearly complete ( $\sim 95\%$ ; Preibisch et al. 2005) down to the stellar mass limit. These X-ray luminosities steadily decrease throughout pre-main-sequence evolution, estimated to follow a time dependence of  $L_x \propto t^{-2/5}$  (Gregory et al. 2016; Johnstone et al. 2021). Together, these results give the functional form given in Equation (1), where  $a$  and  $b$  are constants 30.0 and 1.87 respectively (details noted in Section 2.2 of Wilhelm & Portegies Zwart 2022).

$$L_x(t) = 10^{a+(b*\log[M_*/M_\odot])} \left( \frac{t}{1\text{Myr}} \right)^{-2/5}. \quad (1)$$

In Figure 3, we compare our observed Peter Pan X-ray luminosities with the predictions from Equation (1), assuming main-sequence masses and the nominal ages estimated for the Peter Pan systems in Silverberg et al. (2020). Overall, we find this prescription roughly estimates the locus of our measurements but

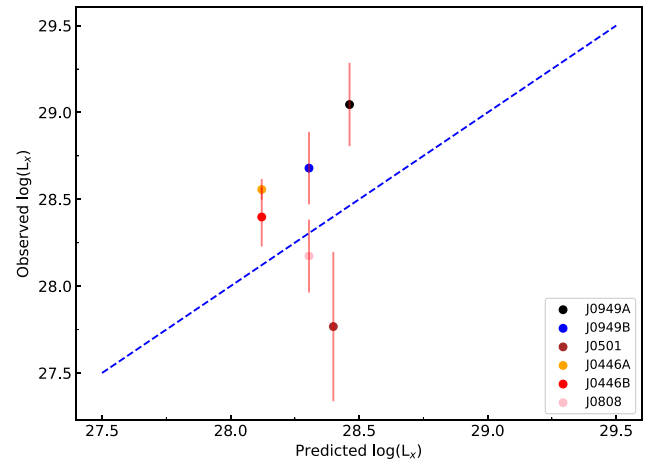


**Figure 3.** Comparison of observed  $L_x$  against the predicted  $L_x$  values used in the recent modeling conducted by Wilhelm & Portegies Zwart (2022; Section 3.3). The dotted line shown represents the 1–1 relation.  $1\sigma$  error bars are shown in light red.

in some cases differs by up to  $\sim 0.5$  dex in the cases of our brightest (J0949A) and faintest (J0501) Peter Pan source. We note however that a more robust comparison is difficult, given the large uncertainties on our derived X-ray luminosities and the small size of our sample. This is further complicated by the large intrinsic scatter in observed stellar X-ray luminosities, varying by factor of  $\sim 2\text{--}3$  as a consequence of variations in surface magnetic activity, magnetic cycles, or flares (Preibisch et al. 2005; Johnstone et al. 2021). Although we find no evidence of flares in our X-ray light-curve data, it remains unclear the extent to which Peter Pan X-ray luminosities are being over- or underpredicted in recent modeling. We discuss the implications of this result and investigate their expected mass-loss rates further in Section 4.1.

## 4. Discussion

Primordial disks are subject to mass loss through a variety of mechanisms, both internal and external to the system (Armitage 2011; Williams & Cieza 2011). In the inner disk, these mechanisms include both the accretion of disk material onto the stellar surface (Hartmann et al. 2016) as well as disk outflows

driven by the high energy flux from the central star, a process known as internal photoevaporation (Hollenbach et al. 1994; Clarke et al. 2001; Alexander et al. 2004; Font et al. 2004; Ercolano et al. 2009; Gorti & Hollenbach 2009; Owen et al. 2010; Williams & Cieza 2011). Photoevaporation is also capable of externally triggering mass loss in the outer disk as a consequence of the far-UV (FUV) radiation from nearby massive stars (Störzner & Hollenbach 1999; Scally & Clarke 2001; Adams et al. 2004; Concha-Ramírez et al. 2019; Winter et al. 2019).

The relative importance of these internal and external channels driving disk dissipation are suspected to depend on stellar mass. Higher mass ( $\gtrsim 1 M_{\odot}$ ) stars have similarly higher levels of accretion (Alexander & Armitage 2006; Alcalá et al. 2014) and suspected internally driven photoevaporation (Owen et al. 2012). These mechanisms likely dominate in this case, given primordial disks around solar-type stars dissipate by  $\sim 10$  Myr regardless of their diverse surrounding environments (Carpenter et al. 2006; Wahhaj et al. 2010; Pecaú & Mamajek 2016). In the lower-mass ( $\lesssim 0.3 M_{\odot}$ ) regime of the Peter Pan stars, the impact of external photoevaporation becomes more comparable even in low external radiation fields (Haworth et al. 2018) given their lower internal accretion. Overall, the relative impact of internal and external mechanisms remain debated for the lowest-mass stars, with these respective class of mechanisms likely dominating disk dispersal at different points of pre-main-sequence evolution (Wilhelm & Portegies Zwart 2022). We discuss the implications of our X-ray results in regards to the described internal and external mechanisms in Sections 4.1 and 4.2, respectively.

#### 4.1. The Impact of Internal Disk Dispersal Mechanisms on Peter Pan Disk Longevity

The overall effect of internal photoevaporation on disk dispersal has remained largely unconstrained, as investigations continue to debate the overall, relative importance of each stellar flux energy regime (e.g., FUV, extreme-ultraviolet (EUV), and X-ray) on resultant mass-loss rates and disk lifetimes. Recent work has argued the impact of EUV radiation is limited, given its absorption over small column densities that does not allow for penetration into the high-density disk midplane (Owen et al. 2010; Picogna et al. 2019). In general, the wind mass-loss predictions from EUV-dominated photoevaporation studies (Hollenbach et al. 1994; Tanaka et al. 2013) have also been lower by 1 order of magnitude or more than that from FUV and X-ray investigations (Ercolano et al. 2009; Gorti & Hollenbach 2009; Owen et al. 2010, 2012; Gorti et al. 2015). Given this and the nature of our observations, we choose to mainly interpret our results in the context of current predictions from X-ray-driven disk photoevaporation modeling.

Wind mass-loss rates from X-ray-driven photoevaporation have been studied in growing detail, with a library of models covering the observed parameter space of both stellar X-ray properties as well as disk metallicity (Picogna et al. 2019; Wölfer et al. 2019). Ercolano et al. (2009) found that the stellar luminosity in the soft (0.1–1 keV) X-ray band drives the bulk of the photoevaporative wind, as harder X-rays are unable to provide enough disk heating to unbind their gaseous components despite deeper penetration (Wang & Goodman 2017; Nakatani et al. 2018). Ercolano et al. (2021) derive a functional form (Equation (2)) for the total expected mass loss from X-ray photoevaporation (given a soft X-ray luminosity down to  $\log L_x \sim 28.5$ ) and find their estimates are in agreement with previous modeling (Owen et al. 2012; Picogna et al. 2019). Prefactor constants have values of  $a_S = -1.947 \times 10^{17}$ ,

**Table 3**  
Mass-loss Rate Estimations

Source	$L_x$ (0.1–1 keV) (erg s <sup>-1</sup> )	$\log(M_{\text{acc}})^a$ (MSun yr <sup>-1</sup> )	$\log(M_w)^b$ (MSun yr <sup>-1</sup> )
J0949A	9.77E+28	-9.3	-7.8
J0949B	2.81E+28	-9.9	-8.2
J0501	4.15E+27	-10.8	-10.2
J0446A	2.12E+28	-10.9	-8.6
J0446B	1.88E+28	-10.6	-8.8
J0808	1.17E+28	-9.75	-9.2

**Notes.**

<sup>a</sup> Estimated in Silverberg et al. (2020) from H $\alpha$  observations.

<sup>b</sup> Computed using the  $\dot{M}_w - L_x$  relation derived by Ercolano et al. (2021) (Equation (2)).

$b_S = -1.572 \times 10^{-4}$ ,  $c_S = -2.866 \times 10^{-1}$ , and  $d_S = -6.694$ , respectively:

$$\log \dot{M}_w(L_{X,\text{soft}}) = a_S \exp\left(\frac{(\ln(\log L_{X,\text{soft}}) - b_S)^2}{c_S}\right) + d_S. \quad (2)$$

Using our best-fit models in the 0.8–3.0 keV band, we extrapolate to determine the 0.1–1.0 keV X-ray luminosities of our Peter Pan sample and calculate their wind mass-loss rates from Equation (2) (as detailed in Ercolano et al. 2021). We report these values in Table 3, conservatively estimating an uncertainty of  $\sim 1$  dex. We find our observed X-ray luminosities predict appreciable wind mass-loss rates that also span a large range (over 2 dex) across our entire sample. We note these values are effectively lower limits given their X-ray luminosities have decreased throughout their pre-main-sequence evolution.

These derived wind loss values track the flow of inner disk material ejected into the outer regions of the disk, in contrast to the ongoing stellar accretion, which funnels inner disk material to the stellar photosphere. As the mass accretion rate decreases and becomes comparable to the wind mass-loss rate, the opening of a gap in the inner disk is expected, clearing the inner disk of material on rapid timescales ( $\lesssim 1$  Myr; Williams & Cieza 2011). We compare our X-ray photoevaporative mass-loss rates to the Peter Pan accretion rates (derived in Silverberg et al. (2020) from H $\alpha$  measurements) to gauge this critical moment of inner disk evolution in Figure 4. Overall, we find X-ray photoevaporative mass-loss rates that are larger than those derived from accretion. Their relative difference could be a consequence of numerous interpretations, which we discuss below.

The relatively low mass-loss rates derived from accretion are not surprising given the Peter Pans represent a sample of fairly evolved low-mass stars. Wilhelm & Portegies Zwart (2022) have shown that lower disk viscosities, which slow the overall accretion, can allow for longer primordial disk lifetimes (upwards of  $\sim 50$  Myr for estimated disk properties around stars of  $\lesssim 0.5 M_{\odot}$ ). However, assuming the rates derived in Equation (2) are correct, these results suggest gaps are expected for all of our Peter Pan systems. The two-component SED fits found for J0808 (Murphy et al. 2018; Flaherty et al. 2019) could be evidence of a gap in a Peter Pan disk supporting this interpretation.

The stronger outliers observed in J0446A/B and J0949A/B are more difficult to explain. We note the greater relative difference in the mass-loss rates for J0446A and J0446B could be evidence of H $\alpha$  emission sourced from stellar activity and

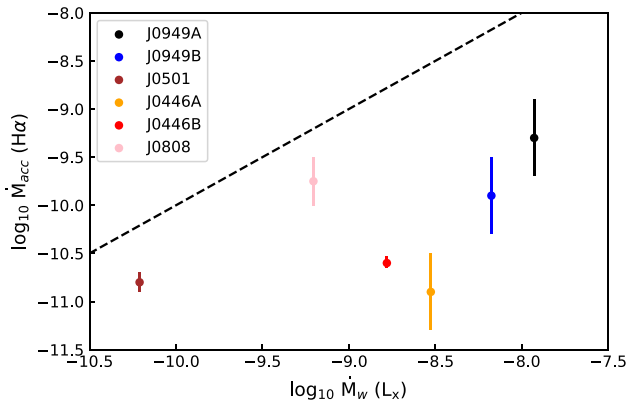


**Figure 4.** Comparison of the expected mass-loss rates between accretion and X-ray-driven photoevaporative disk winds for our Peter Pan sample. Values for the former are reported in Silverberg et al. (2020) while values for the latter are computed from the functional form (Equation (2)) derived in Ercolano et al. (2021). We indicate the 1–1 relation with a black dashed line.

not accretion. These systems exhibited  $H\alpha$  equivalent widths (10–17 Å) and velocity widths (210–240 km s<sup>-1</sup>) that bordered the criteria for an accretion interpretation (Jayawardhana et al. 2003; Fang et al. 2009). While our X-ray results may argue against the Peter Pan status of these systems, this explanation is unable to resolve the tension with J0949A, which is much more clearly accreting given its strong (110 Å) and broad ( $\sim 370$  km s<sup>-1</sup>) emission (Silverberg et al. 2020).

X-ray photoevaporative models predict this disk gap phase occurs at an age of  $\sim 10$ –20 Myr (Ercolano et al. 2021; Picogna et al. 2021) and constitutes the last  $\sim 25\%$  of the disk lifetime (for a stellar X-ray luminosity of  $10^{29}$  erg s<sup>-1</sup>), leading to a quick dispersal of the remaining disk gas in only a few Myr (Ercolano et al. 2021). These short remaining primordial disk lifetimes would be in tension overall with the suspected Peter Pan ages ( $\sim 40$  Myr). Given it is also unlikely to have caught these systems at a point at which X-ray photoevaporative rates have spiked, we argue the  $\dot{M}_w$ – $L_x$  relation found by Ercolano et al. (2021) is likely inaccurate for our Peter Pan sample. The discrepancy may be explained by the fact that our observed Peter Pan luminosity range ( $\log L_x \sim 27.7$ –29.1) extends much lower than the range tested in the models of Ercolano et al. (2021) ( $\log L_x \sim 29$ –31).

Alternatively, our derived X-ray photoevaporative wind mass-loss rates could be overestimated in the case of mechanisms that shield the inner disk from the stellar X-ray radiation. It has been hypothesized that hard X-ray photons could be screened from interacting with the disk via a molecular magnetohydrodynamic inner disk wind, driven by the accretion-powered active stellar magnetic field (Pascucci et al. 2020). This mechanism, however, is mainly predicted for strong classical accretors ( $10^{-8}$  MSun yr<sup>-1</sup>) and is likely inconsistent with early Peter Pan evolution, given their relatively low masses.

Lastly, we note recent findings have suggested younger ages for the Carina and Columba moving groups, ranging from 13 (Booth et al. 2021) to 22 (Schneider et al. 2019) Myr. These ages could reduce the tension in their current classification, given a disk e-folding timescale of  $\sim 4$ –5 Myr (as observed for K-type stars, e.g., Pecauc & Mamajek 2016) which could explain a small fraction of  $\sim 20$  Myr primordial disks. However, these results are in disagreement with the lithium depletion boundary analysis of Murphy et al. (2018), which

indicate a suspected age of  $\sim 40$  Myr for J0808. These younger moving group ages would also not be able to explain the Peter Pan disk candidates identified in other moving groups, such as 2MASS J02265658–5327032 in the  $\sim 45$  Myr Tuc-Hor (Silverberg et al. 2020) moving group and 2MASS J15460752–6258042 in the  $\sim 55$  Myr Argus moving group (Lee et al. 2020). Continued efforts to determine more exact ages for these moving groups are needed.

Overall, our findings question the impact of X-ray photoevaporative disk winds as the primary source of disk dispersal in dM stars. We note photoevaporative winds driven by the host stellar FUV radiation cannot be ruled out from our observations. It has been suspected a large fraction of FUV photons are sourced from the accretion shocks, with a broad range of FUV luminosities ( $10^{-6} L_\odot \lesssim L_{FUV} \lesssim L_\odot$ ) observed in active CTTSs (Gullbring et al. 1998; Yang et al. 2012). Therefore, Peter Pan disks may be a consequence of the low FUV flux incident on the disk of low-mass dM stars given their relatively low levels of accretion over the course of their pre-main-sequence evolution. Future FUV observations of low-mass dM stars will be critical to confirm this behavior. If FUV photoevaporation is indeed critical for dM stars, however, it remains unclear why more Peter Pan disks have yet to be discovered.

#### 4.2. The Impact of External Photoevaporation Mechanisms on Peter Pan Disk Longevity

The intense FUV and EUV fields radiating from the rare, massive O and B stars in a dense star-forming region serve as another source of disk dispersal by driving a photoevaporative wind in the outer circumstellar disk. The overall impact and efficiency of this external mechanism on primordial disk longevity is still currently debated. Previous observational studies of young (1–5 Myr) star-forming regions have found evidence of a correlation between the projected distance to the most luminous ionizing stellar source and the suspected mass of nearby disks in some cases (e.g., Orion Nebula Cluster: Mann et al. 2014; Eisner et al. 2018;  $\sigma$  Orionis: Ansdell et al. 2017; van Terwisga et al. 2019) but not others (e.g., NGC 2024: Mann et al. 2015). Recent *N*-body simulations have not found any evidence of a correlation (Nicholson et al. 2019) even after accounting for projection effects (Parker et al. 2021). Similarly, disk lifetimes were not found to be a function of projected distance to the cluster core in IC 1396 (Silverberg et al. 2021). Even so, these investigations do find that the extreme case of disks in close ( $\sim 0.5$  pc) proximity to massive stars are effectively dissipated, with few disks surviving longer than a few Myr on average.

The evidence of  $\sim 45$  Myr old primordial disk systems in our Peter Pan sample inherently implies significantly low levels of photoevaporation from external radiation for prolonged durations. The investigations of Coleman & Haworth (2020) find primordial disks around low-mass stars could survive up to  $\sim 50$  Myr in the presence of low external radiation fields ( $< 10$  Habing fields ( $1.6 \times 10^{-2}$  erg cm<sup>-2</sup> s<sup>-1</sup>), corresponding to an external photoevaporative mass-loss rate  $\leq 10^{-9} M_\odot$  yr<sup>-1</sup>). A direct quantitative estimation of the local radiation experienced by our Peter Pan systems is not feasible. We note qualitative assessments of the external radiation field, based off of the current 3D positions of the Peter Pan sample relative to other moving group members, are also difficult to interpret. The spatial stellar distribution is not informative of the respective moving group dynamics soon after

**Table 4**  
Nearest Carina Mid-Ms to J0808

Source	R.A. (deg)	Decl. (deg)	SpT	3D Separation <sup>a</sup> (pc)
2MASS J08111195-6656400	122.7996233	-66.94434486	M4.0	8.3
2MASS J08441995-6158424	131.0829793	-61.97836028	M4.9	13.2
2MASS J08122535-6852061	123.1054649	-68.86826186	M7.0	15.5
2MASS J07151705-6555486	108.8210384	-65.93003833	M4.3	17
2MASS J07550342-6717478	118.7641198	-67.29646231	M4.7	19.5

**Note.**

<sup>a</sup> Estimated from Gaia DR3 positions and parallaxes.

formation, times at which the stellar density was higher and close encounters more probable.

Although we are unable to probe these early times ( $\lesssim 2$  Myr), we note the spatial and kinematic properties of Carina, Columba, and Tuc-Hor are somewhat suggestive of unique dynamical evolution, given their fairly large spatial extents ( $\sim 10$ – $15$  pc) and particularly low velocity dispersions ( $\lesssim 1$  km s<sup>-1</sup>) relative to other known moving groups (Gagné et al. 2018). Recent evidence has also suggested that nearby moving groups of stars may be spatially much more extended than previously thought. The high-precision stellar kinematics offered by Gaia DR2 have revealed numerous comoving stellar streams throughout the galaxy at distances ranging 80–1000 pc (Kounkel & Covey 2019). Some of these “Theia” strings have been identified as relatively young ( $\lesssim 100$  Myr) and are suspected to be primordial, reflecting the shape of the molecular cloud from which they have formed. In some cases, these streams appear to be interconnected with nearby moving groups, exhibiting similar estimated isochronal ages and Gaia DR2 UVW space velocities (Gagné et al. 2021). We test for Theia string membership among our Peter Pan sample and note a consistent match with Theia 113 for J0808.

Although the overall dynamical evolution of moving groups and respective Theia strings is still not well understood,  $\sim 2$ – $3$  crossing times are still predicted for the stars in these moving groups. The expectation is then that all moving group members are equally likely to have experienced nearby proximity to massive members, in contrast with an interpretation of strict isolation resulting in low external photoevaporation. The lack of confirmed massive members as assessed by the BANYAN algorithm (Gagné & Faherty 2018) in the moving groups of Carina, Columba, and Tuc-Hor (1 B9 star and no O stars) also argues against the overall impact of external photoevaporation.

If external photoevaporation is most important for disk dispersal in dM stars, we would expect the dM stars nearest the Peter Pan sources to experience similar levels of incident external radiation, and thus also be candidates for harboring long-lived primordial disks. We refer to our list of mid-M stars with high-probability moving group membership (J. Gagné, private communication) to explore this subsample. We find the majority of these candidates did not pass the original criteria of the Disk Detective search (Kuchner et al. 2016) as their disk harboring status could not be determined due to low signal-to-noise ratio WISE observations. We cross-reference this subsample with Gaia DR3 and report the five nearest mid-M stars to the canonical Peter Pan target, J0808, in Table 4. Follow-up near-IR observations of these low-mass stars would help test the extent to which the long-lived disks in our Peter Pan sample could be explained by unusual local, external radiation fields.

Overall, we do not find evidence suggestive of lower external photoevaporation experienced by our Peter Pan sample relative to other moving group members. However, we acknowledge that many of the aspects of both early moving group dynamic and the efficiency of external photoevaporation in the regime of low stellar mass, remain unconstrained. If Peter Pan disk longevity is a consequence of an usually low external FUV radiation field, we predict Peter Pan systems would likely require unusually high amounts of self-shielding during their early evolution to survive to their current suspected ages of 45 Myr and explain their overall rarity.

## 5. Summary and Conclusion

We present new X-ray observations for our sample of six recently identified Peter Pan stars, systems with strong evidence of harboring primordial disks at the advanced ages of  $\sim 45$  Myr. Our results in Section 3 reveal the X-ray characteristics of these sources for the first time. We summarize our main results below.

1. We observe Peter Pan X-ray emission similar to that observed in young, WTTSs (Figure 1). Their derived X-ray luminosities have an overall large dispersion, spanning roughly 1.5 dex ( $\log L_x = 27.7$ – $29.1$ ). We do not find evidence of their X-ray luminosities correlating with their H $\alpha$  equivalent widths, arguing against accretion-driven X-ray suppression being responsible for their extended disk lifetimes.
2. Our derived Peter Pan X-ray luminosities are consistent with that measured for field dM stars of similar spectral type and age (Figure 2). We conclude Peter Pan disk lifetimes are likely not a consequence of central stars with lower  $L_x/L_{\text{bol}}$ .
3. In some cases, our observed X-ray luminosities differ from those used in the recent modeling of Wilhelm & Portegies Zwart (2022) by up to 0.5 dex (Figure 3). It remains unclear the extent to which Peter Pan X-ray luminosities are being over- or underpredicted, given our large measurement uncertainties, overall small sample size, and the large intrinsic scatter in observed X-ray luminosities.
4. Our derived X-ray photoevaporative mass-loss rates (Section 4.1) are in most cases much larger than that estimated by previous H $\alpha$  measurements. These measurements may suggest our Peter Pan systems are in the final phase of their overall disk lifetime, predicted to occur at  $\sim 10$ – $20$  Myr (Ercolano et al. 2021; Picogna et al. 2021). Given the disparity between this timescale and the suspected ages of Peter Pan systems ( $\sim 45$  Myr), we argue the wind mass-loss relation of Ercolano et al. (2021) is inaccurate for

our Peter Pan sample. Overall, these findings call into question the impact of X-ray photoevaporation on disk dispersal for dM stars and may suggest the importance of FUV-driven disk dispersal mechanisms. Given the size of our sample, additional FUV and X-ray observations of low-mass dM stars are needed to help confirm this result.

- Our qualitative assessment of the surrounding Peter Pan environments (Section 4.2) does not predict unusually low levels of external photoevaporation relative to other respective moving group members. However, given this assessment does not inform of early moving group dynamics, the overall impact of external photoevaporation remains unclear. If Peter Pan disk longevity is a consequence of an usually low external FUV radiation field, we predict that Peter Pan systems would likely have to have experienced unusual amounts of self-shielding to explain their current rarity.

This research has made use of the SIMBAD database and the VizieR catalog access tool, operated at CDS, Strasbourg, France. This research has also made use of NASA’s Astrophysics Data System and ds9, a tool for data visualization supported by the Chandra X-ray Science Center (CXC) and the High Energy Astrophysics Science Archive Center (HEASARC) with support from the JWST Mission office at the Space Telescope Science

Institute for 3D visualization. Multiple Python libraries aided the analysis of our data including matplotlib, a Python library for publication quality graphics (Hunter 2007), SciPy (Virtanen et al. 2020), NumPy (Harris et al. 2020), and Astropy, a community-developed core Python package for Astronomy (Astropy Collaboration et al. 2013, 2018). IRAF is distributed by the National Optical Astronomy Observatory, which is operated by the Association of Universities for Research in Astronomy (AURA) under cooperative agreement with the National Science Foundation (Tody 1993). These acknowledgements were compiled using the Astronomy Acknowledgement Generator.

The scientific results reported in this article are based on observations made by the Chandra X-ray Observatory. This research has made use of software provided by the Chandra X-ray Center (CXC) in the application packages CIAO (Fruscione et al. 2006) and Sherpa (Doe et al. 2007).

Facility: CXO (ACIS).

## Appendix A Best-fit Spectral Analysis Models

We describe our spectral fitting procedure in Section 2. The resulting best fits from this analysis are shown in Figures 5–8, respectively. We discuss the derived X-ray properties of our Peter Pan sources in Section 3.

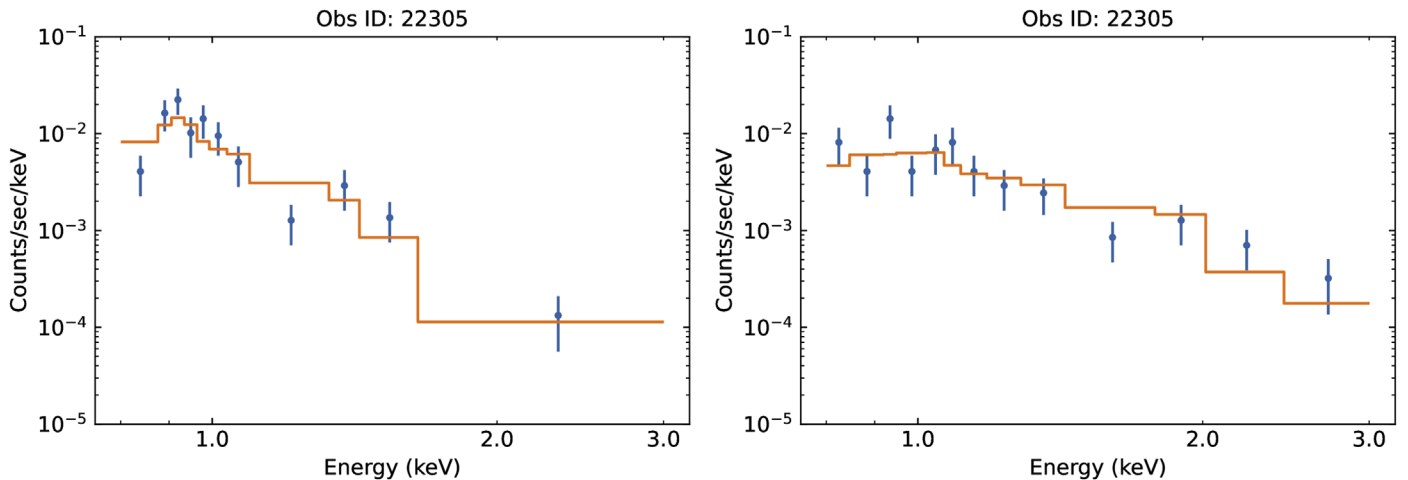


**Figure 5.** Chandra/ACIS X-ray spectra of J0949A (left) and J0949B (right) observed on 2019 December 13. Blue points represent our binned X-ray count data. The orange line represents our best-fit spectral model (see Section 2). The data is fit without binning using the Cstat statistic, but is shown here binned to 5 counts bin<sup>-1</sup> for display purposes (error bars are  $\sqrt{N}$ ) to guide the eye.

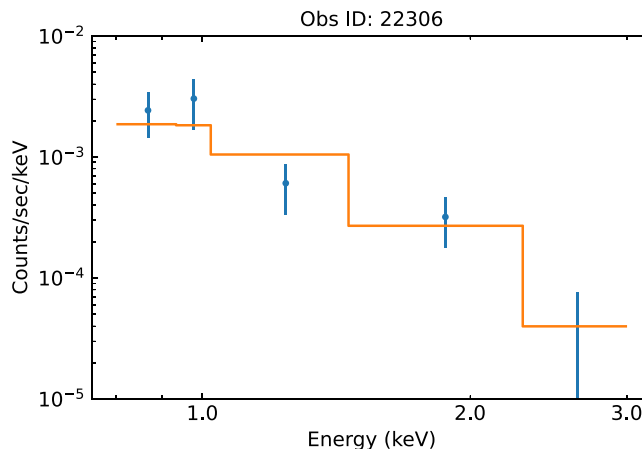


**Figure 6.** Similar to Figure 5, Chandra/ACIS X-ray spectra of J0501 observed on 2019 December 22.



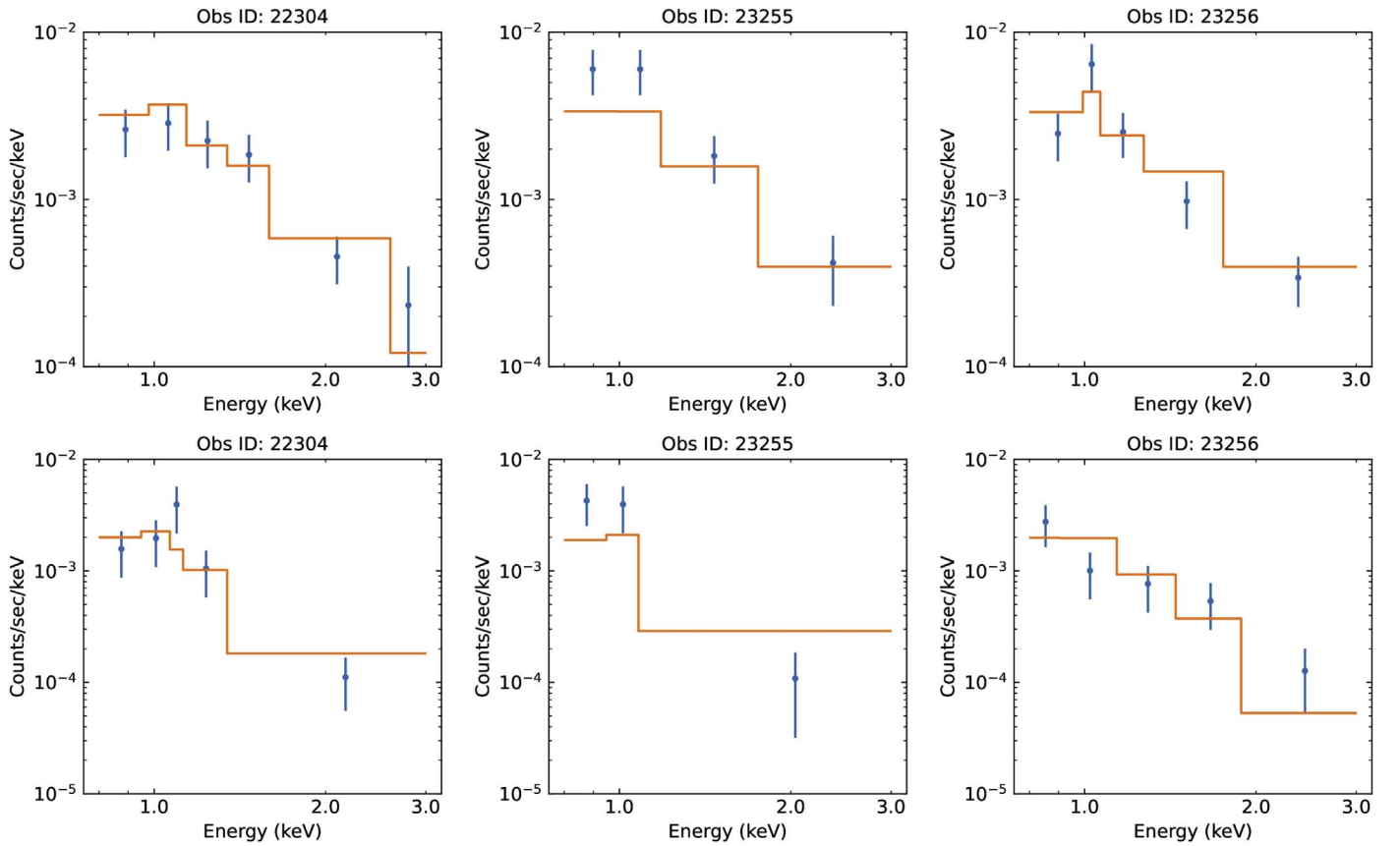


**Figure 7.** Similar to Figure 5, Chandra/ACIS X-ray spectra of J0446A (top row) and J0446B (bottom row) observed on 2020 May 20 (left), 2020 May 21 (middle), and 2020 June 2 (right).

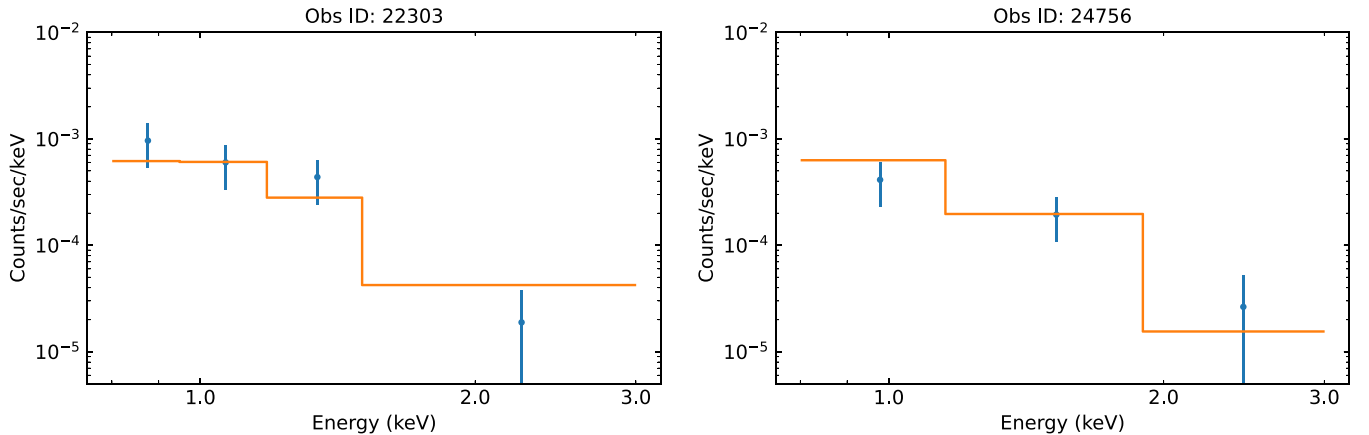


**Figure 8.** Similar to Figure 5, Chandra/ACIS X-ray spectra of J0808 observed on 2021 July 6 (left) and 2021 July 7 (right).

## Appendix B M-star X-Ray Control Sample

To gauge the extent to which the Peter Pan systems are potentially X-ray underluminous, we construct a control sample of objects to compare against. For an appropriate comparison, we only consider objects with suspected spectral types in a similar range as that identified for the Peter Pan sources from Silverberg et al. (2020; i.e., M4–M7). We also require high ( $\gtrsim 95\%$ ) membership probability in the suspected parent moving groups of the identified Peter Pan sources (i.e., Carina, Columba, and Tuc-Hor) as determined by the BAYNAN algorithm (Gagné et al. 2018). These

populations are expected to be coeval with derived ages of  $\sim 45$  Myr (Bell et al. 2015).

For this initial sample of 227 objects (J. Gagné, private communication), we simultaneously query the XMM-Newton Serendipitous Source Catalog (4XMM-DR11) as well as the Chandra Source Catalog (v.2.0) for XMM/Chandra pipeline-derived X-ray fluxes reported by the HEASARC interface. We consider a coordinate search radius of  $5''$  for each object, returning 13 matches. We carefully inspect the X-ray light curves of these matches by eye when available, excluding one source due to an obvious flare feature. To compute X-ray luminosities, we use respective Gaia DR3 distances along with

**Table 5**  
Analog M-star X-Ray Sample








Source	Moving Group <sup>a</sup>	Spectral Type	$L_x$ (erg s <sup>-1</sup> )	log $L_x/L_{\text{bol}}$
2MASS J01275875-6032243	THA	M4	2.30E+28	-3.33
2MASS J02025502-7259155	THA	M5.5	2.87E+28	-3.2
2MASS J02153328-5627175	THA	M4.5	9.14E+27	-3.28
2MASS J03152363-5342539	THA	M5.2	1.90E+28	-3.27
WOH G 312	CAR	M4.6	1.96E+28	-3.42
2MASS J08420090-7113216	CAR	M4.7	1.44E+29	-2.81
2MASS J09421385-5601361	CAR	M4	2.34E+29	-2.63
UCAC3 101-434911	THA	M4	4.06E+28	-3.26
2MASS J23143092-5405313	THA	M5	1.12E+28	-3.3
2MASS J23143092-5405313	THA	M5	4.71E+27	-3.68
2MASS J05360322-6555191	THA	M6.5	3.27E+27	-3.4

**Note.**

<sup>a</sup> The Tuc-Hor and Carina moving groups are estimated to be 45 Myr old (Bell et al. 2015).

the pipeline-derived fluxes listed (EP 8 band for XMM-Newton matches, CSC broadband for Chandra matches). We note these energy ranges (0.2–12 and 0.5–7.0 keV, respectively) do not exactly line up with our reported 0.3–8 keV luminosities. From our best-fit spectral models, we compute our Peter Pan X-ray luminosities in this larger energy band (0.2–12 keV) but find the overall difference is negligible, given the X-ray flux strongly peaks at 1 keV. For this subsample of objects, we also compute bolometric luminosities as indicated in Section 2. We note we do not consider X-ray fluxes derived by ROSAT observations, given its lower overall sensitivity biases detections toward the brightest, X-ray luminous objects. We report the overall X-ray properties of this control sample in Table 5.

**ORCID iDs**

Stefan Laos  <https://orcid.org/0000-0001-8407-2105>  
 John P. Wisniewski  <https://orcid.org/0000-0001-9209-1808>  
 Marc J. Kuchner  <https://orcid.org/0000-0002-2387-5489>  
 Steven M. Silverberg  <https://orcid.org/0000-0002-3741-4181>  
 Hans Moritz Günther  <https://orcid.org/0000-0003-4243-2840>  
 David A. Principe  <https://orcid.org/0000-0002-7939-377X>  
 Marina Kounkel  <https://orcid.org/0000-0002-5365-1267>

**References**

- Adams, F. C., Hollenbach, D., Laughlin, G., & Gorti, U. 2004, *ApJ*, 611, 360  
 Alcalá, J. M., Natta, A., Manara, C. F., et al. 2014, *A&A*, 561, A2  
 Alexander, R. D., & Armitage, P. J. 2006, *ApJL*, 639, L83  
 Alexander, R. D., Clarke, C. J., & Pringle, J. E. 2004, *MNRAS*, 354, 71  
 Ansdell, M., Williams, J. P., Manara, C. F., et al. 2017, *AJ*, 153, 240  
 Armitage, P. J. 2011, *ARA&A*, 49, 195  
 Astropy Collaboration, Robitaille, T. P., Tollerud, E. J., et al. 2013, *A&A*, 558, A33  
 Astropy Collaboration, Price-Whelan, A. M., Sipőcz, B. M., et al. 2018, *AJ*, 156, 123  
 Bell, C. P. M., Mamajek, E. E., & Naylor, T. 2015, *MNRAS*, 454, 593  
 Binks, A. 2016, in IAU Symp. 314, Young Stars Planets Near the Sun, ed. J. H. Kastner, B. Stelzer, & S. A. Metchev (Cambridge: Cambridge Univ. Press), 159  
 Booth, M., del Burgo, C., & Hambaryan, V. V. 2021, *MNRAS*, 500, 5552  
 Boucher, A., Lafrenière, D., Gagné, J., et al. 2016, *ApJ*, 832, 50  
 Carpenter, J. M., Mamajek, E. E., Hillenbrand, L. A., & Meyer, M. R. 2006, *ApJL*, 651, L49  
 Cash, W. 1979, *ApJ*, 228, 939  
 Clarke, C. J., Gendrin, A., & Sotomayor, M. 2001, *MNRAS*, 328, 485  
 Coleman, G. A. L., & Haworth, T. J. 2020, *MNRAS*, 496, L111  
 Concha-Ramírez, F., Wilhelm, M. J. C., Portegies Zwart, S., & Haworth, T. J. 2019, *MNRAS*, 490, 5678  
 Crossfield, I. J. M., Waalkes, W., Newton, E. R., et al. 2019, *ApJL*, 883, L16  
 Demangeon, O. D. S., Zapatero Osorio, M. R., Alibert, Y., et al. 2021, *A&A*, 653, A41  
 Doe, S., Nguyen, D., Stawarz, C., et al. 2007, in ASP Conf. Ser. 376, Astronomical Data Analysis Software and Systems XVI, ed. R. A. Shaw, F. Hill, & D. J. Bell (San Francisco, CA: ASP), 543  
 Eisner, J. A., Arce, H. G., Ballering, N. P., et al. 2018, *ApJ*, 860, 77  
 Ercolano, B., Clarke, C. J., & Drake, J. J. 2009, *ApJ*, 699, 1639  
 Ercolano, B., Picogna, G., Monsch, K., Drake, J. J., & Preibisch, T. 2021, *MNRAS*, 508, 1675  
 Fang, M., van Boekel, R., Wang, W., et al. 2009, *A&A*, 504, 461  
 Flaccomio, E., Micela, G., & Sciortino, S. 2012, *A&A*, 548, A85  
 Flaherty, K., Hughes, A. M., Mamajek, E. E., & Murphy, S. J. 2019, *ApJ*, 872, 92  
 Font, A. S., McCarthy, I. G., Johnstone, D., & Ballantyne, D. R. 2004, *ApJ*, 607, 890  
 Fruscione, A., McDowell, J. C., Allen, G. E., et al. 2006, *Proc. SPIES*, 6270, 62701V  
 Gagné, J., & Faherty, J. K. 2018, *ApJ*, 862, 138  
 Gagné, J., Faherty, J. K., Moranta, L., & Popinchalk, M. 2021, *ApJL*, 915, L29  
 Gagné, J., Mamajek, E. E., Malo, L., et al. 2018, *ApJ*, 856, 23  
 Gaia Collaboration, Brown, A. G. A., Vallenari, A., et al. 2021, *A&A*, 649, A1  
 Getman, K. V., Flaccomio, E., Broos, P. S., et al. 2005, *ApJS*, 160, 319  
 Gillon, M., Triaud, A. H. M. J., Demory, B.-O., et al. 2017, *Natur*, 542, 456  
 Gorti, U., & Hollenbach, D. 2009, *ApJ*, 690, 1539  
 Gorti, U., Hollenbach, D., & Dullemond, C. P. 2015, *ApJ*, 804, 29  
 Grady, C. A., Wisniewski, J. P., Schneider, G., et al. 2020, *ApJL*, 889, L21  
 Gregory, S. G., Adams, F. C., & Davies, C. L. 2016, *MNRAS*, 457, 3836  
 Gullbring, E., Hartmann, L., Briceño, C., & Calvet, N. 1998, *ApJ*, 492, 323  
 Harris, C. R., Millman, K. J., van der Walt, S. J., et al. 2020, *Natur*, 585, 357  
 Hartmann, L., Herczeg, G., & Calvet, N. 2016, *ARA&A*, 54, 135  
 Haworth, T. J., Clarke, C. J., Rahman, W., Winter, A. J., & Facchini, S. 2018, *MNRAS*, 481, 452  
 Hollenbach, D., Johnstone, D., Lizano, S., & Shu, F. 1994, *ApJ*, 428, 654  
 Hunter, J. D. 2007, *CSE*, 9, 90  
 Jayawardhana, R., Mohanty, S., & Basri, G. 2003, *ApJ*, 592, 282  
 Johnstone, C. P., Bartel, M., & Güdel, M. 2021, *A&A*, 649, A96  
 Kastner, J. H., Principe, D. A., Punzi, K., et al. 2016, *AJ*, 152, 3  
 Kounkel, M., & Covey, K. 2019, *AJ*, 158, 122  
 Kuchner, M. J., Silverberg, S. M., Bans, A. S., et al. 2016, *ApJ*, 830, 84  
 Lee, J., Song, I., & Murphy, S. 2020, *MNRAS*, 494, 62  
 Mann, R. K., Andrews, S. M., Eisner, J. A., et al. 2015, *ApJ*, 802, 77  
 Mann, R. K., Di Francesco, J., Johnstone, D., et al. 2014, *ApJ*, 784, 82  
 Murphy, S. J., Mamajek, E. E., & Bell, C. P. M. 2018, *MNRAS*, 476, 3290  
 Nakatani, R., Hosokawa, T., Yoshida, N., Nomura, H., & Kuiper, R. 2018, *ApJ*, 865, 75  
 Nicholson, R. B., Parker, R. J., Church, R. P., et al. 2019, *MNRAS*, 485, 4893  
 Owen, J. E., Clarke, C. J., & Ercolano, B. 2012, *MNRAS*, 422, 1880  
 Owen, J. E., Ercolano, B., Clarke, C. J., & Alexander, R. D. 2010, *MNRAS*, 401, 1415  
 Parker, R. J., Alcock, H. L., Nicholson, R. B., Panić, O., & Goodwin, S. P. 2021, *ApJ*, 913, 95  
 Pascucci, I., Banzatti, A., Gorti, U., et al. 2020, *ApJ*, 903, 78

- Pecaut, M. J., & Mamajek, E. E. 2013, [ApJS](#), **208**, 9
- Pecaut, M. J., & Mamajek, E. E. 2016, [MNRAS](#), **461**, 794
- Picogna, G., Ercolano, B., & Espaillat, C. C. 2021, [MNRAS](#), **508**, 3611
- Picogna, G., Ercolano, B., Owen, J. E., & Weber, M. L. 2019, [MNRAS](#), **487**, 691
- Preibisch, T., Kim, Y.-C., Favata, F., et al. 2005, [ApJS](#), **160**, 401
- Rieke, G. H., Su, K. Y. L., Stansberry, J. A., et al. 2005, [ApJ](#), **620**, 1010
- Scally, A., & Clarke, C. 2001, [MNRAS](#), **325**, 449
- Schneider, A. C., Shkolnik, E. L., Allers, K. N., et al. 2019, [AJ](#), **157**, 234
- Silverberg, S. M., Günther, H. M., Kim, J. S., Arincipe, D. A., & Wolk, S. J. 2021, [AJ](#), **162**, 279
- Silverberg, S. M., Kuchner, M. J., Wisniewski, J. P., et al. 2016, [ApJL](#), **830**, L28
- Silverberg, S. M., Kuchner, M. J., Wisniewski, J. P., et al. 2018, [ApJ](#), **868**, 43
- Silverberg, S. M., Wisniewski, J. P., Kuchner, M. J., et al. 2020, [ApJ](#), **890**, 106
- Skinner, S. L., & Güdel, M. 2013, [ApJ](#), **765**, 3
- Störzer, H., & Hollenbach, D. 1999, [ApJ](#), **515**, 669
- Tanaka, K. E. I., Nakamoto, T., & Omukai, K. 2013, [ApJ](#), **773**, 155
- Telleschi, A., Güdel, M., Briggs, K. R., Audard, M., & Palla, F. 2007, [A&A](#), **468**, 425
- Theissen, C. A., & West, A. A. 2014, [ApJ](#), **794**, 146
- Tody, D. 1993, in ASP Conf. Ser. 52, *Astronomical Data Analysis Software and Systems II*, ed. R. J. Hanisch, R. J. V. Brissenden, & J. Barnes (San Francisco, CA: ASP), 173
- van Terwisga, S. E., Hacar, A., & van Dishoeck, E. F. 2019, [A&A](#), **628**, A85
- Virtanen, P., Gommers, R., Oliphant, T. E., et al. 2020, [NatMe](#), **17**, 261
- Wahhaj, Z., Cieza, L., Koerner, D. W., et al. 2010, [ApJ](#), **724**, 835
- Wang, L., & Goodman, J. 2017, [ApJ](#), **847**, 11
- Wilhelm, M. J. C., & Portegies Zwart, S. 2022, [MNRAS](#), **509**, 44
- Williams, J. P., & Cieza, L. A. 2011, [ARA&A](#), **49**, 67
- Winter, A. J., Clarke, C. J., & Rosotti, G. P. 2019, [MNRAS](#), **485**, 1489
- Wölfer, L., Picogna, G., Ercolano, B., & van Dishoeck, E. F. 2019, [MNRAS](#), **490**, 5596
- Wyatt, M. C. 2008, [ARA&A](#), **46**, 339
- Yang, H., Herczeg, G. J., Linsky, J. L., et al. 2012, [ApJ](#), **744**, 121